Role of Zero-Field Splitting Interactions in the NMR Paramagnetic Relaxation Enhancements Produced by Ni(II)(acac)$_2$(H$_2$O)$_2$

Shawn M. Abernathy and Robert R. Sharp*

Department of Chemistry, The University of Michigan, Ann Arbor, Michigan 48109

Received: January 17, 1997; In Final Form: March 20, 1997[⊗]

Recent theory has predicted that rhombicity in the zero-field splitting (zfs) tensor of transition metal ions with integer spin $S \geq 1$ exerts a strong influence on the NMR- paramagnetic relaxation enhancements (NMR-PRE) of resonances of nuclear spins in solution. ZFS rhombicity induces rapid oscillation in the *z*-component of the electron spin vector, which in the absence of rhombicity, is static with respect to precession or oscillation. Rapid oscillation of S_z acts to decouple the nuclear spin magnetic moment from the local field produced by the electron spin, and in this way profoundly depresses the NMR-PRE. The influence of zfs-rhombicity on the solvent ^{1}H NMR-PRE produced by the complex ion *trans*-bis(2,4-pentanedione)diaquanickel(II) in dioxane solution has been studied by variable field (0.14−8.5 T) T_1 and T_2 measurements. It is shown that the functional form of the T_1 field dispersion profile can be fit by the mathematical expressions of the Zeeman-limit Solomon−Bloembergen−Morgan theory, although the parameters of such a fit are physically meaningless. Spin dynamics simulation methods which account quantitatively for the effects of zfs interactions lead to a very different physical picture of the spin relaxation process, one in which zfs rhombicity is of central importance in determining the functional form of the field dispersion profile.

Introduction

Dissolved paramagnetic species frequently produce large enhancements in the T_1 and T_2 relaxation rates of NMR resonances of nuclear spins on ligands or solvent molecules. This phenomenon, the NMR paramagnetic relaxation enhancement (NMR-PRE), is physically quite different for paramagnetic solutes which possess an electron spin $S \geq 1$ than for $S = 1/2$ species due to the effects of the zero-field splitting (zfs) interactions of the former.[1−8] For $S \geq 1$ species, NMR-PRE behavior can conveniently be discussed with respect to two limiting situations, the Zeeman-limit, where the Zeeman Hamiltonian is much greater than the zfs Hamiltonian ($H_{\text{Zeem}} \gg H_{\text{zfs}}$), and the zfs limit, where $H_{\text{zfs}} \gg H_{\text{Zeem}}$. The nature of the spin precessional motion differs qualitatively in these two limits. In the Zeeman-limit, the precessional motion of the electron spin is quantized along the direction of the external magnetic field $\mathbf{B}_0$, while in the zfs limit, the precessional motion is quantized in the zfs principal axis system. This difference in precessional motion produces large differences in the physical behavior of the NMR-PRE.[9−12]

Theoretical studies[13−16] have indicated that in the zfs-limit the magnitude of the NMR-PRE is particularly sensitive to the presence of rhombic terms in the zfs tensor. The physical origin of this effect, which is described in some detail in refs 12 and 13, can be summarized as follows. The T_1 paramagnetic relaxation enhancement R_{1p} is produced by interaction of the local magnetic field of the electron spin with the magnetic moment of the nuclear spin. Taking the *z*-axis to be the axis of precessional quantization, the local dipolar field associated with S_z is usually much more efficient as a relaxation mechanism than are the dipolar fields associated with S_x and S_y, because the latter are effectively decoupled from the nuclear spin by their rapid precessional motions. In the Zeeman limit, the precessional quantization axis *z* lies along the external magnetic field, and thus the component S_z is, in the usual range of polarizing magnetic field strengths, more effective as an agent of nuclear spin relaxation than are S_x,S_y. In the zfs limit, a similar situation arises except that the electron spin precessional motion is quantized in the zfs-principal axis system (we take $\hat{x},\hat{y},\hat{z}$ as the coordinate axes of the zfs PAS and *x*,*y*,*z* as the coordinate axes of the laboratory frame). When the zfs tensor is uniaxial ($E = 0$), the precessional motion of the electron spin is quantized along the $\hat{z}$-axis. $S_{\hat{z}}$, which is static with respect to precession, provides a more efficient relaxation pathway than do $S_{\hat{x}}$ and $S_{\hat{y}}$ because the latter are precessionally decoupled, as in the Zeeman-limit situation. For integer spins, the presence of rhombic elements in the zfs tensor changes the zfs-limit picture in an important way since zfs rhombicity induces oscillatory motion in $S_{\hat{z}}$, so that all three components of the electron spin may be precessionally decoupled from the nuclear spin. As a result, zfs-rhombicity tends markedly to depress the NMR-PRE relative to the Zeeman-limit or uniaxial zfs-limit situations.

The present study investigates the effects of zfs rhombicity on the T_1 and T_2 field dispersion profiles of the solvent ^{1}H NMR-PRE that is produced by the paramagnetic complex, [Ni(II)(acac)$_2$(H$_2$O)$_2$] (acac = 2,4-pentanedione), in dioxane solution. High-spin Ni(II) is an $S = 1$ ion which has been the subject of numerous experimental and theoretical studies,[17−30] particularly involving the hexaaquanickel(II) cation. The experimental data on [Ni(II)(acac)$_2$(H$_2$O)$_2$] that are reported here have been analyzed using recently developed spin dynamics methods[31] which provide a very general computational platform for computing the NMR-PRE for $S \geq 1$ ions in the presence of arbitrary Zeeman and zfs interactions. The spin dynamics algorithms also account realistically for the effects of Brownian motions, specifically for effects of reorientation of the solute and for translational diffusion of the solute and solvent.

The focus of the present analysis is on examining experimentally various aspects of the available theory for $S \geq 1$ ions, particularly the role of zfs-rhombicity in determining the functional form of the field dispersion profile. The spin dynamics simulations described below show that the magnitude and magnetic field dependence of the NMR-PRE are determined principally, across the experimentally-accessible range of mag-

[⊗] Abstract published in *Advance ACS Abstracts,* May 1, 1997.

S1089-5639(97)00254-5 CCC: $14.00

netic field strengths, by the effects of zfs coupling, particularly by the zfs rhombicity (E) for reasons described above. The effects of the transition in precessional behavior from zfs-type precession at low field to Zeeman-type precession at high field are clearly evident in the data and are the most important determinant of the functional form of the field dispersion profile.

We have also studied systematically the physical information that is derivable from intermolecular NMR-PRE data of this integer spin system. The significant unknown physical parameters which enter the analysis are the zfs D and E parameters and the electron spin relaxation time τ_S; of these, the data depend much more sensitively on E than on D or τ_S for the reasons outlined above. The intermolecular NMR-PRE measurements do not, in themselves, uniquely determine any of the parameters of this set (D, E, τ_S), but they do provide valuable constraints which, when used in conjunction with other types of measurements (e.g., intramolecular NMR-PRE data or temperature-dependent static magnetic susceptibility measurements), would probably do so.

We also show that Zeeman-limit theory which neglects zfs interactions can be parametrized in a manner which permits an approximate fit to the experimental data, even for physical conditions which clearly violate the underlying assumption of the theory, namely $H_{Zeem} > H_{zfs}$. In other words, the mathematical expressions of Zeeman-limit theory are sufficiently flexible in functional form to generate an approximate fit of the data even though the parameters which result from such a fit are physically meaningless. The analysis demonstrates that a proper inclusion of the effects of zfs interactions is essential for interpreting NMR relaxation data in systems of this type.

Experimental Section

The paramagnetic complex [Ni(II)(acac)$_2$(H$_2$O)$_2$], *trans*-bis-(2,4-pentanedione)diaquanickel(II), was synthesized using the method of Charles and Pawlikowski.[32] A 1:2 mole ratio of NiCl$_2$·6H$_2$O to 2,4-pentanedione was added to methanol with stirring. A solution of sodium acetate (same mole quantity as 2,4-pentanedione) in water was added to the above solution. The aquamarine-colored solution was heated, cooled to room temperature, and then refrigerated for several hours. The precipitate was filtered, washed with water, and dried in a vacuum desiccator overnight at room temperature. A 20.0 mM solution of [Ni(II)(acac)$_2$(H$_2$O)$_2$] in 1,4-dioxane containing 0.1% v/v water was prepared. A 200 μL aliquot was transferred to a 10 mm glass tube which had been washed overnight in concentrated sulfuric acid and then rinsed with distilled, deionized water to remove labile paramagnetic ions on the surface. The sample was degassed by four freeze−pump−thaw cycles and sealed under vacuum.

The Ni(II) complex was characterized by IR and magnetic susceptibility measurements, which were in good agreement with the literature.[33,34] The IR spectrum of [Ni(II)(acac)$_2$(H$_2$O)$_2$], which contains a strong water peak at 3400 cm^{-1}, is readily distinguishable from the spectrum of anhydrous [Ni(II)(acac)$_2$], which forms a diamagnetic green trimer in the solid state that is visually distinguishable from the aquamarine-colored monomeric complex, [Ni(II)(acac)$_2$(H$_2$O)$_2$]. To ensure that the procedure used to dry the compound did not produce significant amounts of the anhydrous form, a small quantity of [Ni(II)(acac)$_2$(H$_2$O)$_2$] was heated under vacuum at 90 °C to remove the water ligands. The dehydration yielded the green anhydrous [Ni(II)(acac)$_2$] complex which was characterized by IR. The magnetic moment of [Ni(II)(acac)$_2$(H$_2$O)$_2$] was measured at 23 °C using a magnetic susceptibility balance calibrated with Hg[Co(SCN)$_4$]. A mean value of 3.11 μ_B was calculated for [Ni(II)(acac)$_2$(H$_2$O)$_2$] from three determinations, which deviated from the literature value[34] by 0.6%. This value lies in the expected range for high spin $S = 1$ complexes.

T_1 of the solvent protons was measured in the range (0.14−2.0 T) using a home-built variable field relaxation spectrometer. A modification of the inversion-recovery sequence was used, $(\pi)_\pi - [\tau_\delta - (\pi/2)_0 - \tau_{\tau\rho} - (\pi)_\pi - \tau_{\tau\rho} - (\pi/2)_0]_v$, in which the magnetization was sampled by a triplet sampling sequence at successive intervals τ_d during the decay: the triplet samples the magnetization with a $\pi/2$ pulse, refocuses the magnetization as a spin echo with a phase-shifted π pulse, and then returns the magnetization to the z-axis with a second $\pi/2$ pulse. The reproducibility of this method on a given sample is about ±1.0% as long as $\tau_{tr}/\tau_d \leq 0.01$.[35] T_2 was measured using the CPMG sequence with a pulse spacing of 10 ms. The temperature of the probe maintained at 20.0 ± 0.5 °C with a stream of dry nitrogen. Periodic checks of the measured accuracy and temperature stability were made by comparing the T_1 for degassed sample of pure water to the literature value[36] of 2.95 s at 20.0 °C. T_1 and T_2 at 7.05 and 8.46 T were measured using Bruker AM300 and AM360 high-resolution NMR spectrometers. A 20.0 mM sample of the Ni(II) complex was prepared in 80% dioxane/20% acetone-d_6 containing 0.1% v/v water. The NMR tube was cleaned and the sample degassed as described above. T_1 was measured using the inversion-recovery pulse sequence, and T_2 was measured from the solvent proton line width. The temperature of the probe was maintained at 20 ± 1 °C.

Theory

The Zeeman-limit NMR-PRE was calculated as previously[10] using the expressions

$$R_{1p} = (\gamma_I g\beta)^2\left(\frac{\mu_0}{4\pi}\right)^2 S(S+1)\left(\frac{4\pi}{15}\right)[7J_F(\omega_S) + 3J_F(\omega_I)] \quad (1)$$

$$R_{2p} = (\gamma_I g\beta)^2\left(\frac{\mu_0}{4\pi}\right)^2 S(S+1)\left(\frac{2\pi}{15}\right)[4J_F(0) + 13J_F(\omega_S) + 3J_F(\omega_I)] \quad (2)$$

where γ_I is the nuclear magnetogyric ratio, g is the electron g-factor (assumed to be 2), β is the Bohr magneton, μ_0 is the magnetic permeability of free space, and S is the electron spin quantum number. $J_F(\omega)$ is the spectral density function of Hwang and Freed[37,38]

$$J_F(\omega) = \frac{8}{27}\frac{N}{dD_t}\mathrm{Re}\left[\frac{1 + \frac{1}{4}\chi(\omega)^{1/2}}{1 + \chi(\omega)^{1/2} + \frac{4}{9}\chi(\omega) + \frac{1}{9}\chi(\omega)3/2}\right] \quad (3)$$

where $\chi(\omega) = (i\omega\tau_D + \tau_D/\tau_S)$. Equations 1 and 2 assume that $\omega_S \gg \omega_I$, where ω_S and ω_I are Larmor precession frequencies of the electron and nuclear spins. τ_D is a translational correlation time

$$\tau_D = d^2/(D_1 + D_2) \quad (4)$$

where d is the distance of closest approach of the I and S spins, D_1 and D_2 are self-diffusion coefficients of the solvent and solute, $\tau_r = \tau_R^{(1)}$ is the reorientational correlation time for a molecule-fixed vector, and τ_S is the electron spin relaxation time. In the Zeeman limit, electron spin relaxation is in general field dependent and, for $S \geq 1$, a multiexponential process. Following Bloembergen and Morgan[17] and McLachlan[39], eq 5 was used for the average electron spin relaxation rate produced by random fluctuation of the zfs tensor:

$$\left\langle \frac{1}{\tau_S} \right\rangle = \frac{1}{\tau_S^{(0)}} \left(\frac{0.2}{1 + \omega_S{}^2 \tau_v{}^2} + \frac{0.8}{1 + 4\omega_S{}^2 \tau_v{}^2} \right) \quad (5)$$

$$\frac{1}{\tau_S^{(0)}} = (\Delta^2/5)\,\{4S(S+1) - 3\}\tau_v \quad (6)$$

$$\Delta^2 = (2\pi c)^2[(2/3)(D')^2 + 2(E')^2] \quad (7)$$

$(\tau_S^{(0)})^{-1}$ is the low-field limiting value of the electron spin relaxation rate, D' and E' are parameters of the dynamic zfs tensor, τ_v is the correlation time for zfs fluctuations, and c is the speed of light.

NMR-paramagnetic relaxation enhancements were also calculated by means of spin dynamics simulations using methods which are described elsewhere[31] and implemented in the program SpinDyn.f. The algorithms of this program compute the time-correlation function of the magnetic dipole−dipole coupling in a time domain calculation using the quantum mechanical equation of motion of the electron spin operators. The electron spin Hamiltonian $H_S(t)$ employed in the equation of motion is composed of Zeeman and quadratic zfs (D and E) terms of arbitrary magnitude, and the algorithms of the program model stochastic fluctuations in $H_S(t)$ by a small step simulation of isotropic Brownian reorientation. The effects of translational diffusion are described by the time correlation function of Torrey[40] and Abragam.[41]

SpinDyn.f treats the electron spin relaxation rate $\tau_S{}^{-1}$ as a sum of contributions

$$\frac{1}{\tau_S} = \frac{1}{\tau_{S,v}} + \frac{1}{\tau_{S,r}} \quad (8)$$

where $\tau_{S,v}$ describes spin relaxation due to collisional modulation of the zfs tensor, for which the correlation time is τ_v, and $\tau_{S,r}$ describes relaxation produced by Brownian reorientation of the static zfs tensor. SpinDyn.f computes the latter contribution directly by simulation of the spin motion in the time domain under the influence of a spin Hamiltonian $H_S(t)$, which contains stochastic time dependence due to reorientational modulation of the zfs term, and thus the introduction of a parameter $\tau_{S,r}$ is not required. $\tau_{S,v}$ was calculated using eqs 5−7.

The level splitting ω_S in eq 5 equals the Zeeman splitting ω_S only in the high-field limit; in the uniaxial zfs limit the level splitting equals the static zfs splitting, $\omega_D = 2\pi cD$. A detailed theory of the magnetic field dependence of $\tau_{S,v}$ that is appropriate to the zfs limit is not currently available. In the slow-motion low-field limiting situation for $S = 1$, $\tau_S{}^{-1}$ presumably has contributions at the three zfs transition frequencies, $2\omega_E$ and $\omega_D \pm \omega_E$. When $H_Z \geq H_{zfs}$, the transition frequencies become field dependent, approaching ω_S and $2\omega_S$ in the Zeeman limit (where eqs 5−7 are valid). Lacking appropriate theory for $\tau_{S,v}$ in the slow-motion zfs limit and in the intermediate regime, we have described $\tau_{S,v}{}^{-1}$ by an expression of the form of eq 5 but with the quantity $\omega_n = ((n\omega_S)^2 + \omega_D{}^2)^{1/2}$ in place of $n\omega_S$. $\tau_{S,v}^{(0)}$ is then defined as the low-field limiting value of $\tau_{S,v}$, rather than by eq 6. This description of the magnetic field dependence of $\tau_{S,v}$ is not necessarily very accurate, but it provides correct limiting behavior at high and low magnetic field strengths, and it ensures that $\tau_{S,v}$ varies monotonically between these limits. It will be shown below that the magnetic field dependence of $\tau_{S,v}$ is not a sensitive parameter of theory for the $S = 1$ spin system studied here.

Results

Solvent ^{1}H NMR paramagnetic relaxation enhancements, R_{1p} and R_{2p}, were measured for a 20.0 mM solution [Ni(II)(acac)$_2$(H$_2$O)$_2$] in dioxane over a range of magnetic field strengths 0.14−8.46 T at a temperature of 20 °C. The results are shown in Figure 1. Within experimental uncertainty, $R_{1p} = R_{2p}$ across this range of temperature and magnetic field strength, except for the points above 7 T.

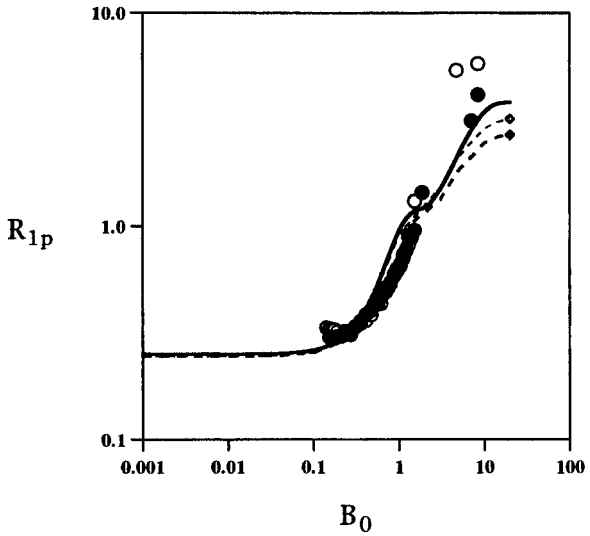

Figure 1. Comparison of Zeeman-limit calculations (solid and dashed lines) with experimental R_{1p} (filled circles) and R_{2p} (open circles) data for a 20.0 mM solution of [Ni(II)(acac)$_2$(H$_2$O)$_2$] in dioxane at 20 °C. R_{1p} and R_{2p} in s^{-1} are plotted against field strength B_0 in tesla. Results of Zeeman-limit calculations using analytical theory are shown for R_{1p} (filled diamonds, dashed line) and R_{2p} (open diamonds, dashed line). The solid curve was generated by spin dynamics simulation. In the calculations, the self-diffusion coefficients of the solvent and solute were taken to be $D_1 = 1.4 \times 10^{-9}$ and $D_2 = 4.1 \times 10^{-10}$ m^2 s^{-1}, respectively, and the distance of closest approach was $d = 0.4$ nm. The molecular reorientation time of the solute was set to $\tau_R^{(1)} = 3.33 \times 10^{-10}$ s. The parameters $\tau_{S,v}^{(0)}$ and τ_v were 5.0×10^{-13} and 6.5×10^{-12} s, respectively.

Theoretical fits to these data were initially carried out using Zeeman-limit theory (eqs 1−8). The distance of closest approach d in eqs 3 and 4 was estimated from a radial distribution function generated by molecular dynamics simulation of the [Ni(II)(acac)$_2$(H$_2$O)$_2$]/dioxane solution, performed using the Dynamics Simulations Module of the Cerius[2] Molecular Modeling software package (Biosym-Molecular Simulations, Inc.). The simulations were performed under constant NVE conditions with a unit cell containing 20 molecules of dioxane plus a single [Ni(II)(acac)$_2$(H$_2$O)$_2$] complex, assuming periodic boundary conditions. The unit cell dimensions were chosen to give the proper solution density. The bond lengths of [Ni(II)(acac)$_2$(H$_2$O)$_2$] were taken from the X-ray crystal structure[42] and constrained to remain constant during the simulation. Output from the program was generated in the form of a radial distribution function $g(r)$ of Ni−H distances (Figure 2). Both intramolecular and intermolecular Ni−H distances are present in g(r), and peaks corresponding to the intramolecular distances are indicated in the figure. Based on the simulated radial distribution function, an effective "distance of closest approach" of solvent protons to the Ni(II) ion was estimated to be 4.0 ± 0.2 Å. This value was taken to be somewhat larger than the smallest observed distances because of the nonspherical coordination environment of the Ni(II) ion. The self-diffusion coefficient of dioxane was taken from the literature,[43] $D_1 = 1.4 \times 10^{-9}$ m^2 s^{-1}, and the self-diffusion coefficient and reorientational correlation time of [Ni(II)(acac)$_2$(H$_2$O)$_2$] were calculated from Stokes−Einstein theory to be $D_2 = 4.1 \times 10^{-10}$ m^2 s^{-1} and $\tau_R^{(1)} = 3.33 \times 10^{-10}$ s, respectively, using the measured[44] viscosity for dioxane at 20 °C of 1.308×10^{-3} kg m^{-1} s^{-1}.

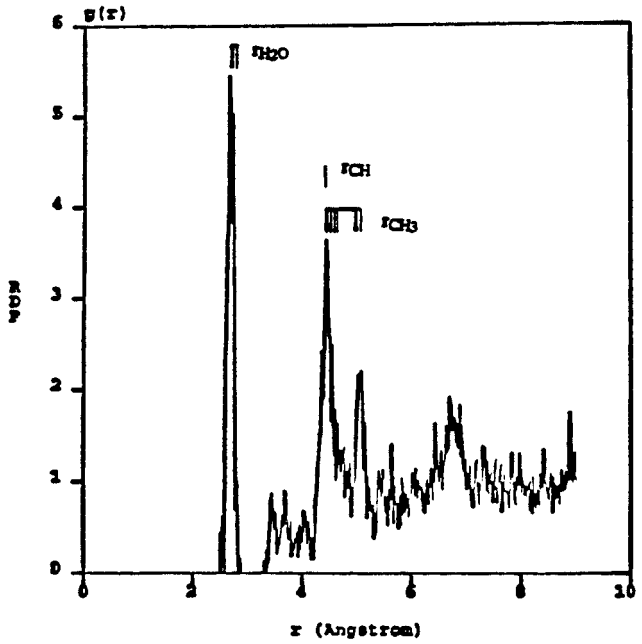

Figure 2. Radial distribution function $g(r)$ of the Ni−H distance for the various hydrogen-containing entities of the $[Ni(II)(acac)_2(H_2O)_2]$ complex. $g(r)$ was generated using the dynamic Simulations Module of the Cerius[2] Molecular Modeling software package (BioSym-Molecular Simulations, Inc.) as described in the text. Intramolecular Ni−H distances are specified in the figure.

The solid and dashed curves in Figure 1 show the results of spin dynamics simulations (solid curve) and analytical theory (dashed curves) computed using Zeeman-limit assumptions. In these fits, the distance of closest approach d and the parameters describing the molecular dynamics ($D_1 + D_2$, $\tau_R^{(1)}$) were calculated as described above and held fixed during the simulation. With these quantities fixed, only $\tau_S^{(0)}$ and τ_v remain as variable parameters of the theory. τ_v has negligible influence in the low-field region where $\omega_S\tau_v \ll 1$, and thus the magnitude of R_{1p} at low field determines $\tau_S^{(0)}$, for which the value $\tau_S^{(0)} = 0.50$ ps was found. The rise of R_{1p} with increasing field strength is due physically, in Zeeman-limit theory, to magnetic field dependence in τ_S, and the functional form of the rise determines τ_v, which was found to be 6.5 ps. Clearly the overall fit using these parameters is rather poor, and the finding that $\tau_v \gg \tau_S$ clearly indicates that the Zeeman-limit Redfield theory, which underlies eqs 6−8, is inappropriate. In addition, the fitted value of is $\tau_S^{(0)}$ exceedingly short. We show below that the Zeeman-limit values of both this quantity and τ_v very probably lack physical significance.

A series of spin dynamics simulations were then performed to investigate the influence of zfs interactions on the properties of the field dispersion profile. Figures 3−7 show the results of a series of spin dynamics simulations in which $\tau_{S,v}^{(0)}$ was set to a relatively long value, $\tau_{S,v}^{(0)} = 20$ ps, with $\tau_v = 2$ ps. Holding these two parameters constant, the effect on the field dispersion profile due to variations in D and in the E/D ratio was explored. In Figure 3, D was set equal to 1 cm^{-1} and the E/D ratio was varied from 0 to 0.3 (1/3 being the maximum value of the E/D ratio; higher ratios correspond physically to relabeling the axes, doubling the value of D, and changing its sign). Figure 4 shows a similar set of simulations but with $D = 5$ cm^{-1}. This figure illustrates the extreme sensitivity of R_{1p} to zfs rhombicity when D is substantial. Figure 5 shows similar simulations with $D = 8.0$ cm^{-1} and $E/D = 0.0$, 0.03, 0.05, and 0.08, respectively. The last of these curves provides an accurate fit of the data. Positive values of D and E were used in the calculations, but the NMR-PRE is independent of the signs of the zfs parameters.

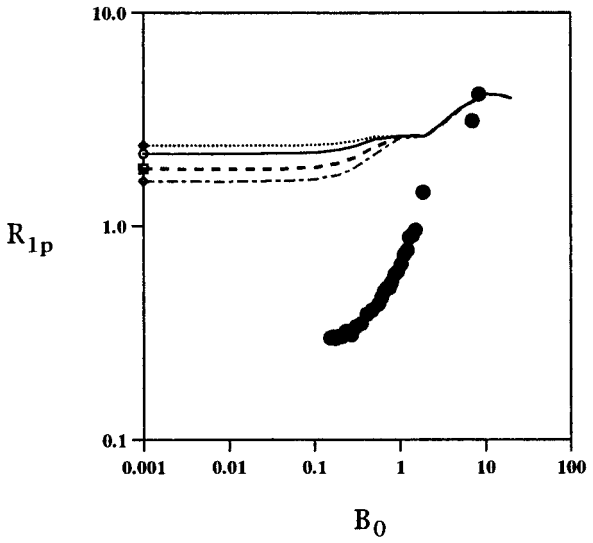

Figure 3. Comparison of spin dynamics simulations with R_{1p} field dispersion profile data (filled circles). Calculations assumed $D = 1.0$ cm^{-1} with $E/D = 0.0$ (filled diamond, dotted curve), 0.1 (open circle, thin solid curve), 0.2 (half-filled square, bold dashed curve), and 0.3 (half-filled diamond, dashed curve). Other molecular parameters are given in the legend of Figure 1.

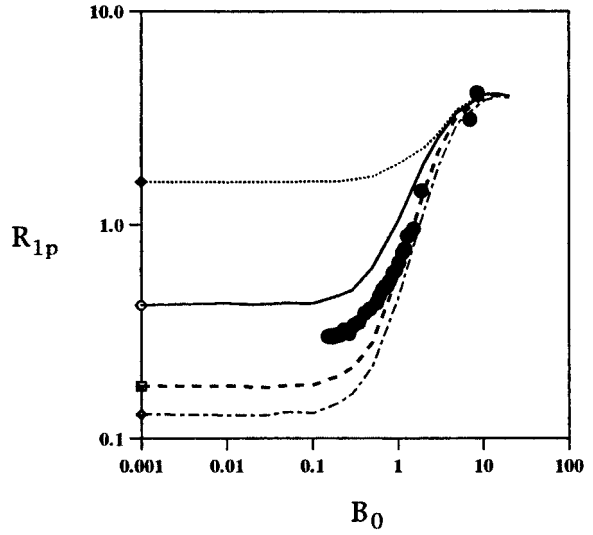

Figure 4. Comparison of spin dynamics simulations with experimental field dispersion profile data (filled circles). Conditions were as described in the legend of Figure 3 except $D = 5.0$ cm^{-1}.

The transition of precessional quantization behavior from zfs-type precession to Zeeman-type precession occurs in the vicinity of the magnetic field strength at which $\omega_S = \omega_D = 2\pi cD$. For $S = 1$, this condition occurs at field strengths near $B_{tr} \approx 1.1$ D, where B_{tr} is in tesla and D is in cm^{-1}. Thus the steep rise in the simulated field dispersion profiles in the neighborhood of 1 T results physically from the transition from zfs-type to Zeeman-type precession. It is evident from the spin dynamics simulations that the presence of significant zfs rhombicity profoundly depresses the field dispersion profile in the zfs limit and intermediate regimes for the reasons described above. In the Zeeman-limit regime the curves coalesce, becoming independent of D and E.

The intermolecular field dispersion profiles do not in themselves determine unique values of D and E, even when $\tau_{S,v}^{(0)}$ and τ_v are fixed. In Figure 6, three simulations performed with rather different sets of D and E are compared with experimental data and shown to produce fits of very similar quality. The

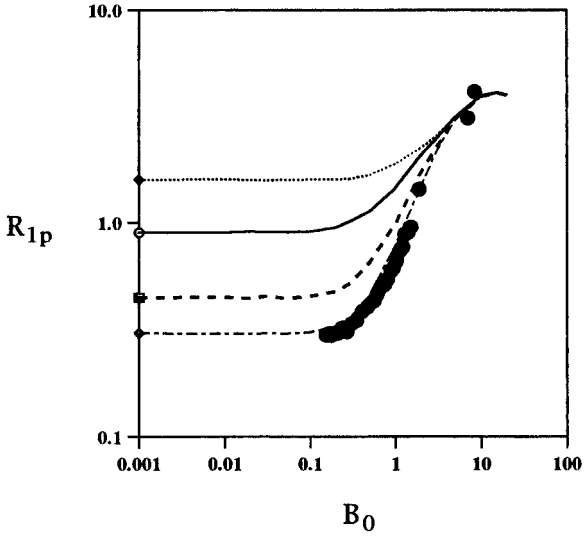

Figure 5. Comparison of spin dynamics simulations with experimental field dispersion profile data (filled circles). Conditions were as described in the legend of Figure 3 except $D = 8.0$ cm^{-1}, $E/D = 0.0$ (filled diamond, dotted curve), 0.03 (open circle, thin solid curve), 0.06 (half-filled square, bold dashed curve), and 0.08 (half-filled diamond, dashed curve).

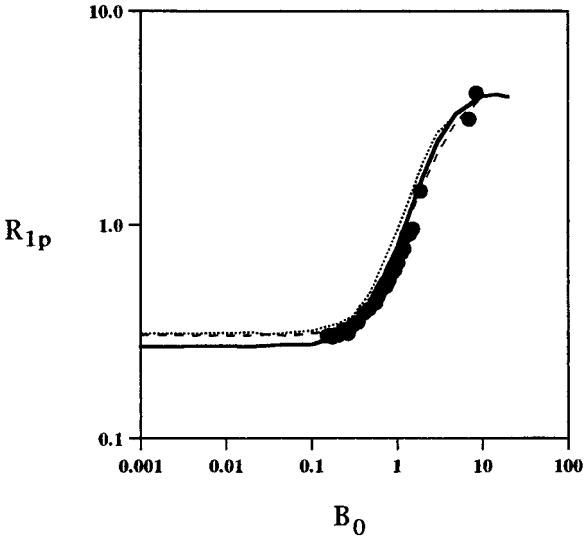

Figure 6. Comparison of spin dynamics fits with experimental field dispersion profile data (filled circles) in the zfs limit. The simulations were done assuming $D = 3.0$ cm^{-1}, $E/D = 0.32$ (dotted curve); $D = 5.0$ cm^{-1}, $E/D = 0.14$ (bold solid curve); and 8.0 cm^{-1}, $E/D = 0.08$ (dashed curve). Other parameters are given in the legend of Figure 3.

three sets are (1) $D = 3.0$ cm^{-1}, $E = 0.96$ cm^{-1}; (2) $D = 5.0$ cm^{-1}, $E = 0.70$ cm^{-1}; (3) $D = 8.0$ cm^{-1}, $E = 0.64$ cm^{-1} (all with $\tau_{S,v}^{(0)} = 20$ ps and $\tau_v = 2$ ps). While the field dispersion profile data do not uniquely determine D and E, they provide important constraints on the possible values of these parameters. A number of fits like those in Figure 6 (i.e., with similar goodness of fit) were performed, and Figure 7 shows a plot of the D and E values which produced fits of acceptable quality. Acceptable fits could be produced with D in the range 3 cm^{-1} $\leq D$ and E in the range 0.60 cm^{-1} $\leq E \leq$ 1.0 cm^{-1}. In addition to this range information, the data provide a relationship between the acceptable values of D and E, such that if D were known from another experiment (for example, from a fit to variable temperature magnetic susceptibility data), then E would be known fairly accurately.

In addition to the dependence on D and E, the field dispersion profiles also depend on $\tau_{S,v}^{(0)}$ and τ_v, though much less strongly. Figure 8 shows the effect of a 5-fold variation in $\tau_{S,v}^{(0)}$ and

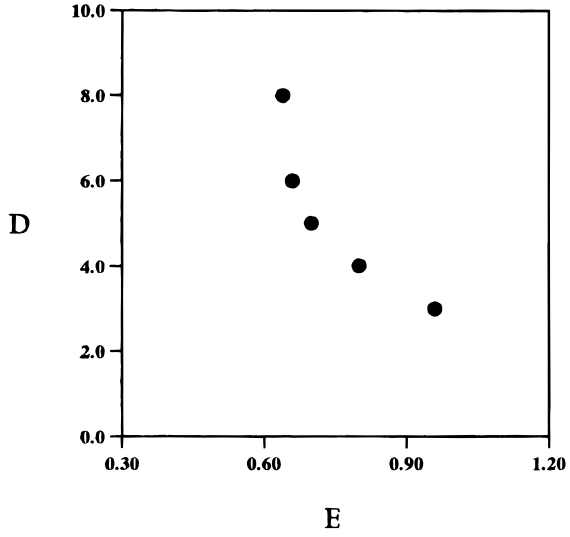

Figure 7. D and E values providing acceptable fits to the experimental field dispersion profile. Other parameters are the same as in the legend of Figure 3.

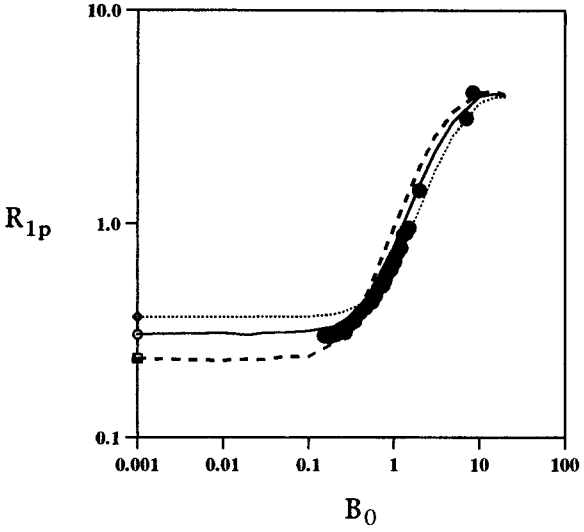

Figure 8. Dependence of spin dynamics fits on $\tau_{S,v}^{(0)}$. Spin dynamics simulations assumed $D = 8.0$ cm^{-1}, $E/D = 0.08$, and $\tau_v = 2$ ps, with $\tau_{S,v}^{(0)}$ 10 ps (half-filled diamond, dotted curve), 20 ps (open circle, solid curve), and 50 ps (half-filled square, dashed curve). Other conditions are as given in the legend of Figure 3.

Figure 9 the effect of a 5-fold variation in τ_v, in each case with the other three parameters held fixed. τ_v influences the field dispersion profile only at relatively high field strengths (Figure 10). Its value, though not very well defined by the data, clearly lies in the vicinity of 2 ps rather than 7.5 ps, the value inferred from the Zeeman-limit fit of Figure 1.

Discussion

These results show that the pronounced rise observed in R_{1p}, which in Zeeman-limit theory is described as the result of the magnetic field dependence of τ_S, can be modeled with equal or better accuracy in an entirely different physical picture as the effect of competing zfs and Zeeman interactions in the electron spin Hamiltonian. In particular, large rhombicity (E/D) in the zfs tensor profoundly depresses R_{1p} in the zfs-limit regime, and this depression disappears when the Hamiltonian changes from the zfs to the Zeeman-limit situation. The rise in the field dispersion profile that accompanies the transition from zfs-type electron spin precessional motion to Zeeman-type precessional motion is the main qualitative feature of the experimental data.

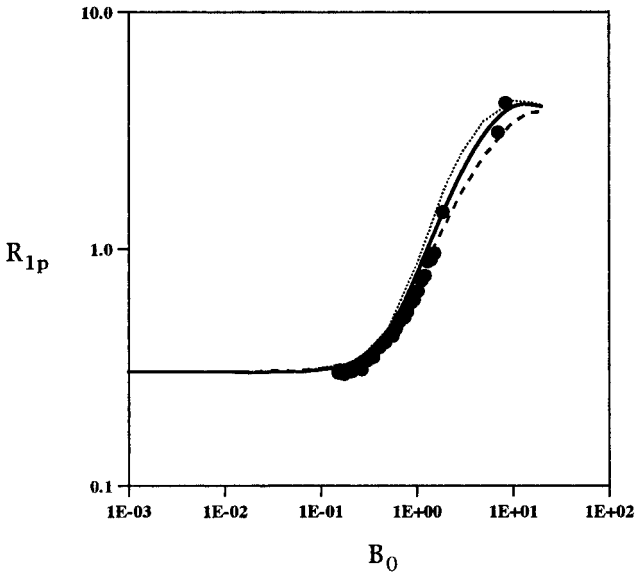

Figure 9. Dependence of spin dynamics simulations on τ_v. Simulations assumed $D = 8.0$ cm^{-1}, $E/D = 0.08$, and $\tau_{S,v}^{(0)} = 20$ ps, with $\tau_v = 1$ ps (bold dashed curve), 2 ps (bold solid curve), and 5 ps (dotted curve). Other conditions are as given in the legend of Figure 3.

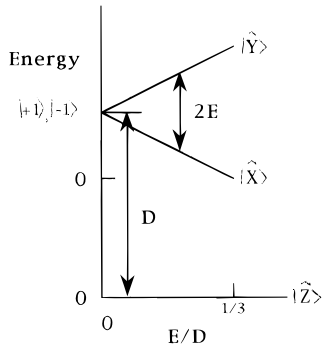

Figure 10. Energy level diagram of a $S = 1$ spin system in the zfs limit. The diagram is a plot of the energy against rhombicity (E/D).

The influence of zfs rhombicity on the NMR-PRE, for which quantitative analytical theory appropriate to the slow-motion zfs-limit situation has been developed previously,[14,15] results from the oscillatory motion which zfs rhombicity induces in S_z. It is worth stressing in this regard that both the coherent and stochastic motions of the electron−nuclear dipole−dipole interaction exert a profound influence on the nuclear spin relaxation. The rate of energy transfer between the I and S spin systems depends on the Fourier component of the dipolar magnetic field of S that is at resonance with the nuclear spin I. The power density associated with each component of $\bar{S}$ ($S_{x,y,z}$) is a Lorentzian band of width $2/\tau_c$ (where τ_c is the I−S dipole−dipole correlation time) centered on the precessional frequency of that component. Thus in the Zeeman limit, S_z produces a Lorentzian continuum of dipolar power of width $2/\tau_c$ that is centered at $\omega = 0$ (since S_z is precessionally static). The frequency component at ω_I produces the NMR-PRE due to S_z. In the uniaxial zfs limit, $S_{\hat{z}}$ (the component of $\bar{S}$ along the $\hat{z}$-axis of the zfs-PAS) produces a Lorentzian band of width $2/\tau_c$ centered at $\omega = 0$ (since in this case $S_{\hat{z}}$ is precessionally static). In the rhombic zfs situation, $S_{\hat{z}}$ oscillates at frequency $2\omega_E$, so that the Lorentzian spectral density bands are displaced to $\pm 2\omega_E$. When $2\omega_E\tau_c \geq 1$, the oscillation of $S_{\hat{z}}$ shifts the power density due to $S_{\hat{z}}$ away from ω_I, thereby suppressing the NMR-PRE.

This picture can be made more quantitative with the aid of Figure 10, which shows the energy level diagram in the zfs limit for $S = 1$, plotted against rhombicity (E/D), where both E and D have been taken as positive. The eigenstates of H_{zfs} transform under D_{2h} (the point group of the zfs Hamiltonian) as $\hat{x}$, $\hat{y}$, and $\hat{z}$ and are labeled accordingly. In the uniaxial zfs limit ($E = 0$), the eigenfunctions $|\hat{x}\rangle$, $|\hat{y}\rangle$, $|\hat{z}\rangle$ correlate with the circularly polarized functions $|+1\rangle$, $|0>$, $|-1>$, where the latter set are the eigenfunctions both of the uniaxial zfs Hamiltonian and of the Zeeman Hamiltonian when the external magnetic field is aligned along $\hat{z}$. It is shown in ref 13 that $S_{\hat{z}}$ oscillates at the eigenfrequency $\omega_E = 4\pi cE$ corresponding to the splitting of $|x\rangle$ and $|\hat{y}\rangle$. In the uniaxial zfs limit, $|\hat{x}\rangle$ and $|\hat{y}\rangle$ are degenerate and $S_{\hat{z}}$ is a constant of the motion. In this situation, the local dipolar field associated with $S_{\hat{z}}$ has substantial low-frequency Fourier components at the nuclear Larmor frequency ω_I, and the nuclear spin relaxation pathway provided by $S_{\hat{z}}$ is relatively efficient. The oscillation of $S_{\hat{z}}$ which occurs when $|E| > 0$ acts to decouple $S_{\hat{z}}$ from the nuclear spin, thereby lowering the efficiency of spin relaxation. When $H_{Zeem} \gg H_{zfs}$, the electron spin precession is quantized along the z-axis of the laboratory frame, and the component S_z provides an efficient relaxation pathway. Thus the intermediate regime where $H_{zfs} \approx H_{Zeem}$ is expected to be a region of dramatically increasing relaxation efficiency when $|E| > 0$. This region of changing precessional character is clearly apparent in the experimental field dispersion profile for $[Ni(II)(acac)_2(H_2O)_2]$.

The fit to the data depends significantly on the values of four parameters: $|D|$, $|E|$, $\tau_{S,v}^{(0)}$, and τ_v. Of these, $|E|$ has the greatest influence on the simulation. Its value, though not unambiguously determined by the experimental data, is constrained to lie within the range $0.60 \leq |E| \leq 1.0$ cm^{-1}. The value of $|D|$ has very little influence on the fit if $|D| \geq 5$ cm^{-1} and a minor influence on the fit when $|D|$ is in the range, 3 cm^{-1} $< |D| <$ 5 cm^{-1}. Values of $|D|$ much below about 3 cm^{-1} are inconsistent with the data if, as we have assumed (see below), $\tau_{S,v}^{(0)} \geq 10$ ps. Measured values of D have been reported[45,46] for a number of near-tetragonal Ni(II) complexes of the type [*trans*-$Ni(II)L_4X_2$], where L = pyrazole or 5-methylpyrazole and X = Cl^-, Br^-, I^-, NO_3^-, the values ranging between 2.5 and 10.5 cm^{-1}. As shown in Figure 7, values of $|D|$ within this range are consistent with the NMR-PRE data for $[Ni(II)(acac)_2(H_2O)_2]$ if $\tau_{S,v}^{(0)} \geq 10$ ps. The intermolecular solvent NMR-PRE data alone do not uniquely determine the set of unknown theoretical parameters $|D|$, $|E|$, $\tau_{S,v}^{(0)}$, and τ_v, but the constraints provided by the data, if used in conjunction with the results of other experiments (e.g., intramolecular NMR-PRE data, temperature-dependent static magnetic susceptibility data, low temperature heat capacity data), would probably do so.

It is shown in Figure 1 that the Zeeman-limit picture also provides at least a rough fit to the experimental data, although for several reasons it appears that the Zeeman-limit analysis is not realistic. Both the experimental studies cited above[1,2] and *ab initio* quantum mechanical calculations[47,48] involving distorted octahedral Ni(II) complexes have indicated that the zfs interaction is the order of several cm^{-1}, in which case zfs-effects cannot appropriately be ignored at magnetic field strengths less than at least several tesla.

In addition, the exceedingly short τ_S values (*ca.* 0.5 ps) that are implied by Zeeman-limit theory cannot meaningfully be interpreted in terms of spin relaxation phenomena. A 0.5 ps time scale implies extremely rapid spin motion corresponding, by way of comparison, to 1 radian of precessional motion of an electron spin in an external magnetic field of 11 T (for $g = 2$), or 1 radian of zfs-type precessional motion when $D = 10$ cm^{-1}. In the zfs limit, spin motion on this time scale implies the presence of off-diagonal terms of H_{zfs} which are at least the order of 10 cm^{-1}. Also, if $\tau_v \gg \tau_{S,v}$ as implied by the Zeeman-limit fit, then the zfs interaction would effectively be static over time intervals comparable to $\tau_{S,v}$, in which case the electron

spin motion would need to be computed as a coherent motion driven by a static zfs Hamiltonian (as is done by SpinDyn.f), rather than by a rapidly fluctuating zfs Hamiltonian as in Redfield theory. From these considerations it is clear that the motion which produces the very small observed R_{1p} value is not electron spin "relaxation" (i.e., stochastic transitions between the eigenstates of the spin system), but rather coherent oscillatory motion of $S_{\hat{z}}$ that is induced by the static zfs rhombicity, and that the critical parameter of theory is the static zfs E parameter (and to a much smaller extent D), rather than the parameter Δ^2 in eq 7, which describes stochastic fluctuations of the zfs tensor.

In the spin dynamics fits we have assumed that the true electron spin relaxation time $\tau_{S,v}^{(0)}$ is much longer than the 0.5 ps Zeeman-limit value and is instead the order of 10 ps or longer. A similar order of magnitude of $\tau_{S,v}^{(0)}$ has been inferred for the $Ni(H_2O)_6^{2+}$ cation, which however represents a rather different physical situation since in this case the static zfs tensor vanishes. Electron spin relaxation times of order 10 ps have previously been inferred[10,15] from a zfs-limit analysis of NMR-PRE data for [Mn(III)$(acac)_3$], which is an integer ($S = 2$) spin system. In this complex, the static zfs tensor is approximately uniaxial ($D = 3.1$ cm^{-1}, $E/D \ll 1/3$) because of the strong tetragonal Jahn−Teller elongation that is characteristic of Mn(III). From eq 7, the $S = 2$ Mn(III) ion is relaxed (21/5) times more efficiently than the $S = 1$ Ni(II) ion, τ_v and Δ^2 being equal. Thus the measured value of $\tau_{S,v}^{(0)} = 10$ ps for [Mn(III)$(acac)_3$] suggests that $\tau_{S,v}^{(0)}$ for [Ni(II)$(acac)_2(H_2O)_2$] is probably at least 10 ps and is almost certainly much longer than 0.5 ps.

The very large influence of zfs rhombicity on the NMR-PRE described above seems also to be present in other Ni(II)-containing systems where the Ni^{II} coordination geometry is lower than octahedral. T_1 relaxometry data for the $Ni(H_2O)_6^{2+}$ cation and for the Ni^{2+} cation solvated by ethylene glycol (Ni^{II}(eg)) provide an interesting comparison in this regard.[22] The molar relaxivity of Ni^{II}(eg) is an order of magnitude lower than that of $Ni(H_2O)_6^{2+}$; also, a pronounced increase in the NMR-PRE with increasing magnetic field strength, similar to that exhibited by the field dispersion profile of [Ni(II)$(acac)_2(H_2O)_2$] in Figure 1, occurs at field values that are an order of magnitude lower for Ni^{II}(eg) (*ca.* 0.5 T) than for $Ni(H_2O)_6^{2+}$ (*ca.* 5 T). Based on a Redfield interpretation for τ_S (eqs 5−7), this difference has been attributed[1,22] to order of magnitude differences in $\tau_{S,v}^{(0)}$ and τ_v, with the value of $\tau_{S,v}^{(0)}$ much shorter and the value of τ_v much longer for Ni^{II}(eg) than for $Ni(H_2O)_6^{2+}$. In view of the analysis of the preceding section, however, the situation for Ni^{II}(eg) appears to be similar physically to that for [Ni(II)$(acac)_2(H_2O)_2$]. Thus it seems likely that the pronounced depression of R_{1p} at low field results from effects of static zfs rhombicity and that the pronounced rise in the field dispersion profile for $B_0 > 0.5$ T results from the transition from zfs-type to Zeeman-type precession. Behavior similar to that of [Ni(II)$(acac)_2(H_2O)_2$] and Ni^{II}(eg) has also been reported[1] for Ni(II)−carbonic anhydrase, suggesting that in this case also zfs rhombicity is probably the determining factor.

Acknowledgment. This research was supported by the U.S. National Science Foundation in the form of a research grant, CHE-9423351. S.M.A. received financial support in the form of a Rackham Merit Fellowship from the University of Michigan.

References and Notes

(1) Banci, L.; Bertini, I.; Luchinat, C. *Nuclear and Electron Relaxation*; VCH Publishers: Weinheim, Germany; 1991; pp 134−135.
(2) Pegg, D. T.; Doddrell, D. M. *Aust. J. Chem.* **1978**, *31*, 475.
(3) Benetis, N.; Kowalewski, J.; Nordenskiold, L.; Wennerstrom, H.; Westlund, P.-O. *Mol. Phys.* **1983**, *48*, 329.
(4) Benetis, N.; Kowalewski, J.; Nordenskiold, L.; Wennerstrom, H.; Westlund, P.-O. *J. Magn. Reson.* **1984**, *58*, 261.
(5) Benetis, N.; Kowalewski, J. *J. Magn. Reson.* **1985**, *65*, 13.
(6) Bertini, I.; Luchinat, C.; Mancini, M.; Spina, G. *J. Magn. Reson.* **1984**, *59*, 213.
(7) Bertini, I.; Luchinat, C.; Kowalewski, J. *J. Magn. Reson.* **1985**, *62*, 235.
(8) Banci, L.; Bertini, I.; Briganti, F.; Luchinat, C. *J. Magn. Reson.* **1986**, *66*, 58.
(9) Sharp, R. R. *J. Chem. Phys.* **1990**, *93*, 6921.
(10) Bayburt, T.; Sharp, R. R. *J. Chem. Phys.* **1990**, *92*, 5892.
(11) Sharp, R. R. *J. Magn. Reson.* **1992**, *100*, 491.
(12) Sharp, R. R. *J. Chem. Phys.* **1993**, *98*, 912.
(13) Fukui, H.; Miura, K.; Matsuda, H. *J. Magn. Reson.* **1990**, *88*, 311.
(14) Sharp, R. R. *J. Chem. Phys.* **1993**, *98*, 2507.
(15) Bovet, J.-M.; Sharp, R. R. **1993**, *99*, 18.
(16) Bertini, I.; Galas, O.; Luchinat, C.; Parigi, G. J. *Magn. Reson.* **1995**, *A113*, 151.
(17) Bloembergen, N.; Morgan, L. O. *J. Chem. Phys.* **1961**, *34*, 842.
(18) Friedman, H. L.; Holz, M.; Hertz, H. G. *J. Chem. Phys.* **1979**, *70*, 3369.
(19) Kowalewski, J.; Laaksonen, A.; Nordenskiold, L.; Blomberg, M. *J. Chem. Phys.* **1981**, *74*, 2927.
(20) Benetis, N.; Kowalewski, J.; Nordenskiold, L.; Edlund, U. *J. Magn. Reson.* **1984**, *58*, 282.
(21) Hertz, H. G.; Holz, M. *J. Magn. Reson.* **1985**, *63*, 64.
(22) Banci, L.; Bertini, I.; Luchinat, C. *Inorg. Chim. Acta* **1985**, *100*, 173.
(23) Westlund, P.-O.; Benetis, N.; Wennerstrom, H. *Mol. Phys.* **1987**, *61*, 177.
(24) Kowalewski, J.; Larsson, T.; Westlund, P.-O. *J. Magn. Reson.* **1987**, *74*, 56.
(25) Larsson, T.; Kowalewski, J. *Magn. Reson. Chem.* **1988**, *26*, 1020.
(26) Westlund, P.-O.; Larsson, P. T. *Acta Chem. Scand.* **1991**, *45*, 11.
(27) Larsson, T.; Westlund, P.-O.; Kowalewski, J.; Koenig, S. H. *J. Chem. Phys.* **1994**, *101*, 1116.
(28) Odelius, M.; Ribbing, C.; Kowalewski, J. *J. Chem. Phys.* **1995**, *103*, 1800.
(29) Svoboda, J.; Nilsson, T.; Kowalewski, J.; Westlund, P.-O.; Larsson, P. T. *J. Magn. Reson.* **1996**, *121*, 108.
(30) Odelius, M.; Ribbing, C.; Kowalewski, J. *J. Chem. Phys.* **1996**, *104*, 3181.
(31) Abernathy, S. M.; Sharp, R. R. *J. Chem. Phys.*, submitted for publication.
(32) Charles, R. G.; Pawlikowski, M. A. *J. Phys. Chem.* **1958**, *62*, 440.
(33) Alison, M. A.; Bennett, G. A.; Fowlds; Thompson, D. A. *Polyhedron* **1989**, *8*, 2305.
(34) Cotton, F. A.; Fackler, J. P., Jr. *J. Am. Chem. Soc.* **1961**, *83*, 2818.
(35) Haddy, A. E.; Frasch, W. D.; Sharp, R. R. *Biochemistry* **1985**, *24*, 7926.
(36) Simpson, J. H.; Carr, H. Y. *Phys. Rev.* **1958**, *111*, 1201.
(37) Hwang, L.-P.; Freed, J. H. *J. Chem. Phys.* **1975**, *63*, 4017.
(38) Freed, J. H. *J. Chem. Phys.* **1978**, *68*, 4034.
(39) McLachlan, A. D. *Molec. Phys.* **1964**, *7*, 271.
(40) Torrey, H. C. *Phys. Rev.* **1953**, *92*, 962.
(41) Abragam, A. *The Principles of Nuclear Magnetism*; Oxford University: Oxford, U.K.; 1961; pp 300−302.
(42) Montgomery, H.; Lingafelter, E. C. *Acta Crystallogr.* **1964**, *17* 1481.
(43) Claessens, M.; Fiasse, P.; Fabre, O.; Zimmermann, D.; Reisse, J. *Nouv. J. Chim.* **1984**, *8*, 357.
(44) Geddes, J. A. *J. Am. Chem. Soc.* **1933**, *55*, 4832.
(45) Klaaijsen, F. W.; Reedijk, J.; Witteveen, H. T. *Z. Naturforsch.* **1972**, *27A*, 1532.
(46) Vermaas, A.; Groeneveld, W. L.; Reeddijk, J. *Z. Naturforsch.* **1977**, *32A*, 632.
(47) Ribbing, C.; Odelius, M.; Kowalewski, J.; Pettersson, L. *Theor. Chim. Acta* **1994**, *87*, 307.
(48) Ribbing, C.; Odelius, M.; Laaksonen, A.; Kowalewski, J.; Roos, B. **1990**, *24*, 295.
(49) Sharp, R. R.; Abernathy, S. M.; Lohr, L. L. Manuscript in preparation.